J Therm Anal Calorim (2010) 99:21–26
DOI 10.1007/s10973-009-0531-4

Size effect of silica nanoparticles on thermal decomposition of PMMA

D. Q. Zou · H. Yoshida

Japan Symposium 2008

Abstract The size effect of silica nanoparticles (SiO_2) on thermal decomposition of poly(methylmethacrylate) (PMMA) was investigated by the controlled rate thermogravimetry. Thermal degradation temperature of PMMA–SiO_2 composites depended on both fraction and size of SiO_2, the thermal degradation temperature of 23 nm (diameter) SiO_2–PMMA (6.1 wt%) was 13.5 °C higher than that of PMMA. The thermal stabilities of 17 nm SiO_2–PMMA (3.2 wt%) and 13 nm SiO_2–PMMA (4.8 wt%) were 21 and 23 °C, respectively, higher than that of PMMA without SiO_2. The degree of degradation improvement was increased linearly with the surface area of SiO_2. The number of surface hydroxyl group in unit volume of SiO_2 particle increased with increasing the specific surface area of SiO_2, and the interaction between hydroxide group of SiO_2 and carbonyl group of PMMA had an important role to improve the thermal stability of PMMA.

Keywords Thermal decomposition · Silica nano-particles · Poly(methylmethacrylate) (PMMA) · Specific surface area · Controlled rate thermogravimetry (CRTG) · Small-angle X-ray scattering (SAXS)

Introduction

Polymer nano-composites consisted of polymer and inorganic nano-materials have good advantages both in physical and thermal properties. Poly(methylmethacrylate) (PMMA) and silica (SiO_2) nano-particle composites prepared by the sol–gel process [1] and the in situ polymerization [2, 3] show the improvement of thermal stability. These PMMA–SiO_2 nano-composites have chemical linkages between PMMA and SiO_2. On the other hand, PMMA–SiO_2 nano-composite prepared by physical blend also shows the improvement of physical and thermal properties [4–7]. However, the improvement of properties depends on the sample preparation and the character of SiO_2 used. Only 1 wt% of 12 nm SiO_2 particle improved the thermal stability of PMMA nanocomposite prepared by solvent-casting method, and the dimensional stability improved by adding more than 20 wt% of SiO_2 [5].

We have reported the thermal stability of PMMA–SiO_2 nano-composites prepared by solvent-casting method was improved about 14 °C at 6 wt% fraction of 23 nm SiO_2 [8]. As the thermal stability improvement by SiO_2 was disturbed the steric hindrance of ester group, the interaction between carbonyl groups of ester groups in PMMA and hydroxyl groups of SiO_2 surface had an important role to improve the thermal stability [8]. In this study, the effects of SiO_2 particle size and fraction on the thermal stability improvement of PMMA–SiO_2 nano-composites were investigated by controlled rate thermogravimetry (CRTG).

Experiments

Materials

PMMA ($Mw = 1.2 \times 10^5$, $Mw/Mn = 2.3$), prepared by the solid-state radical polymerization, were used through this experiments. Three silica (SiO_2) nano-particles (Rhodia Co., Ltd., Italy, average particle sizes 13, 17, 23 nm) were used.

D. Q. Zou · H. Yoshida (✉)
Graduate school of Urban Environmental Science,
Tokyo Metropolitan University, 1-1 Minamioosawa Hachioji,
Tokyo 192-0397, Japan
e-mail: yoshida-hirohisa@tmu.ac.jp

After drying SiO_2 at 125 °C for 12 h under vacuum, SiO_2 nano-particles were dispersed in THF under nitrogen atmosphere. Then polymer sample was added in the SiO_2-dispersed THF, and the mixed solution was stirred over night. The SiO_2 mass fraction (ϕ_{SiO_2}) in PMMA was determined by the residue at 600 °C. PMMA–SiO_2 composites were obtained by solvent casting and dried under reduced pressure at 140 °C for 12 h.

Measurements

The surface analysis of SiO_2 was investigated by FTIR method using a JASCO FT/IR-620 with surface-reflection optics. Accumulation time and wave number resolution of FTIR measurement were 64 times and 2 cm^{-1}, respectively.

Specific surface area measurement of SiO_2 was carried out using Shimadzu-TriStar 3000 with BET method by N_2 absorption. Before the determinations, the samples were pretreated by heating to 200 °C in vacuum in order to remove adsorbed species. The pretreatments took 20–24 h to ensure complete gas desorption.

Thermogravimetric measurement of SiO_2 (3–4 mg) was using TG–DTA (Seiko Instruments, TG-DTA6200) at 10 °C min^{-1} from room temperature to 800 °C under air flow (200 mL min^{-1}). The evolved gas analysis was carried out by the combined TG–FTIR method. Thermogravimetric measurements of PMMA–SiO_2 composites were carried out using TG–DTA (Seiko Instruments, Tokyo, Japan, TG-DTA6200) under air flow (200 mL min^{-1}) condition from room temperature to 600 °C at a constant scanning rate mode (10 °C min^{-1}) and a constant mass loss rate mode (CRTG). CRTG measurements of nano-composites (3–4 mg) were carried out at 5–6 μg min^{-1} of mass loss rate.

Small-angle X-ray scattering (SAXS) experiments of PMMA and PMMA–SiO_2 composites were performed at 25 °C using the SAXS optics at the beam line 10C, Photon Factory, High Energy Accelerator Research Organization, Tsukuba, Japan. The wavelength of X-ray (λ) used was 0.15 nm. The accumulation time of SAXS measurement was 300 s. The scattering vector $(q = (4\pi \sin\theta)/\lambda)$ was covered from 0.02 to 5 nm^{-1}, 2θ was the scattering angle.

Results and discussion

CRTG results of PMMA and PMMA–SiO_2 composites with different particle sizes were shown in Fig. 1. Under oxidative condition, the mass loss of PMMA completed at 420 °C, the total mass of SiO_2 nano-particles dispersed in PMMA was experimentally determined from the residue at 600 °C. With increasing ϕ_{SiO_2}, the mass loss temperature shifted to higher temperature side for all PMMA–SiO_2 composites. The ϕ_{SiO_2} value which showed the highest mass loss temperature was depended on the size of SiO_2 particle. The mass loss temperature, $T_{d(CRTG)}$, was determined by the extrapolation of CRTG curve as shown in Fig. 1a.

The $T_{d(CRTG)}$ values were plotted against ϕ_{SiO_2} in Fig. 2 for PMMA–SiO_2 composites with different particle sizes: (a) 23, (b) 17, and (c) 13 nm. The $T_{d(CRTG)}$ of PMMA without SiO_2 was 265.8 °C, the $T_{d(CRTG)}$ increased 13 °C for the PMMA–SiO_2 (23 nm) composite with 2% of ϕ_{SiO_2}. For the PMMA–SiO_2 (23 nm) composite, the maximum $T_{d(CRTG)}$ value was observed at 6% of ϕ_{SiO_2}, where the $T_{d(CRTG)}$ value was 13.5 °C higher than that of pure PMMA. The $T_{d(CRTG)}$ value decreased gradually for PMMA–SiO_2 composite over 6% of ϕ_{SiO_2}; however, the $T_{d(CRTG)}$ value of PMMA–SiO_2 composite (18%) was 7 °C higher than that of pure PMMA.

The dispersed SiO_2 acted as an inhibiter of thermal degradation of PMMA. The similar SiO_2 fraction dependency on the thermal stability improvement was observed for other PMMA–SiO_2 composites with different SiO_2 particle sizes. The maximum $T_{d(CRTG)}$ value for the PMMA–SiO_2 (17 nm) composite was observed at 3.2% of ϕ_{SiO_2}, where the degradation temperature was 21 °C higher than that of pure PMMA. Similar to PMMA–SiO_2 (23 nm) composite, the $T_{d(CRTG)}$ value decreased gradually for PMMA–SiO_2 (17 nm) composite over 3.2% of ϕ_{SiO_2}; however, the $T_{d(CRTG)}$ value of PMMA–SiO_2 composite (18%) was 15 °C higher than that of PMMA. The maximum $T_{d(CRTG)}$ value of the PMMA–SiO_2 (13 nm) composite was observed at 4.8% of ϕ_{SiO_2}, where the degradation temperature was 23 °C higher than pure PMMA. The thermal stability improvement of PMMA–SiO_2 composites depended on the particle size of SiO_2, and the maximum $T_{d(CRTG)}$ values were observed at the ϕ_{SiO_2}, ranging from 2 to 8%.

The CRTG curves indicated that the mass loss of PMMA occurred at two steps, the first step occurred at a constant mass loss rate in the temperature range from 260 to 270 °C, and the second step continued after the first step until 420 °C. The second step consisted of several reactions with various mass loss rates. The first step degradation was caused by de-polymerization of PMMA, which was confirmed by the evolved gas analysis using TG–FTIR method [8]. The relative mass loss in the first and the second steps were 70 and 30% of total mass, respectively, for PMMA without SiO_2. The similar two-step mass loss process was observed for PMMA–SiO_2 composites. The first step degradation of PMMA–SiO_2 composites shifted to higher temperature and the relative mass loss in the first step increased with the increase in ϕ_{SiO_2}. The relative mass loss occurred in the first step of degradation was plotted against ϕ_{SiO_2} for all PMMA–SiO_2 composites in Fig. 3, which showed the similar ϕ_{SiO_2} dependency of $T_{d(CRTG)}$ shown in Fig. 2. The maximum mass loss was observed in the ϕ_{SiO_2}

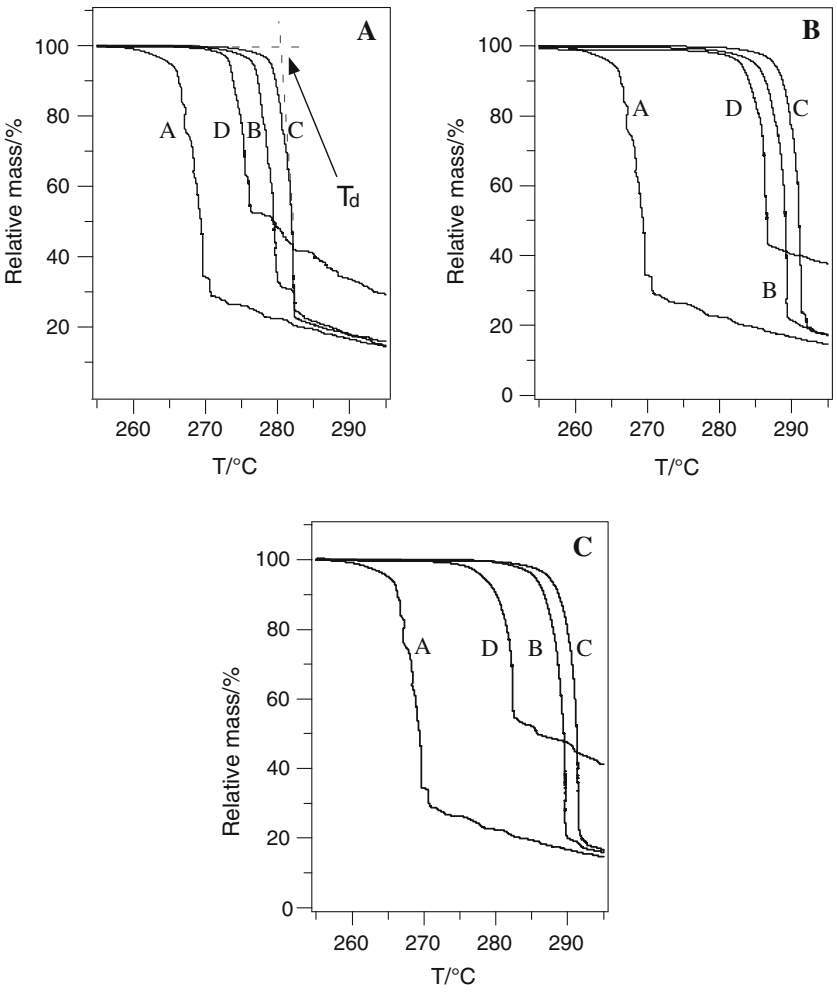

Fig. 1 Relative mass loss curves of PMMA and PMMA–SiO_2 (23 nm) composites (**a**) (*A* PMMA, *B* 0.9%, *C* 6.1%, *D* 18%), PMMA–SiO_2 (17 nm) composites (**b**) (*A* PMMA, *B* 2.2%, *C* 3.2%, *D* 16.3%), PMMA–SiO_2 (13 nm) composites (**c**) (*A* PMMA, *B* 0.5%, *C* 4.8%, *D* 17.6%) with various mass fraction of SiO_2 obtained by CRTG under air condition

range, where the maximum $T_{d(CRTG)}$ was observed for each PMMA–SiO_2 composites. With the increase in $T_{d(CRTG)}$, the first step mass loss increased as functions of SiO_2 fraction and size. These facts indicated that the SiO_2 particles acted as an inhibiter of the first step thermal degradation of PMMA.

The thermal degradation temperature of PMMA–SiO_2 composites increased with increasing SiO_2 fraction, and then decreased after the maximum, which appeared in the ϕ_{SiO_2} range at around 2–8 wt%. The SiO_2 particle size influenced the thermal stability improvement of PMMA, the maximum $T_{d(CRTG)}$ value increased with decreasing the particle size. With decreasing the size of particles, particles prefer to form aggregates, and the homogeneous dispersion of particles becomes difficult with the increase in particle fraction in polymers.

The normalized SAXS profiles of PMMA and PMMA–SiO_2 composites (17 nm) were shown in Fig. 4. The SAXS profiles of PMMA–SiO_2 composites showed the scattering peaks at $q = 0.2$ and 0.9 nm^{-1}. The observed SAXS profile, $I(q)_{obs}$, was described as follows:

$$I(q)_{obs} = I(q)_{PMMA} + I(q)_{SiO_2} \quad (1)$$

Here, $I(q)_{PMMA}$ and $I(q)_{SiO_2}$ indicate SAXS profiles from PMMA and SiO_2, respectively. From the X-ray scattering theory [9], $I(q)_{SiO_2}$ is evaluated by the following equation:

$$I(q)_{SiO_2} = n_p \int_0^\infty P(q,R)S(q,R_{eff})f(R)dR \quad (2)$$

Here, n_p, R, $P(q, R)$, $S(q, R)$, and $f(R)$ are the average number density of particles, the radius of particle, the form factor, the structure factor of system, and the distribution of particles, respectively.

$$P(q)_{SiO_2} = \left[(\rho_{SiO_2} - \rho_{PMMA})(R_{SiO_2})^3 F(q,R_{SiO_2})\right]^2 \quad (3)$$

$$F(q,R_{SiO_2}) = 3\left\{[\sin(qR_i) - (qR_i)\cos(qR_i)]/(qR_i)^3\right\} \quad (4)$$

Here, ρ_i indicates the scattering electron density of PMMA and SiO_2.

The SAXS profile fitting was carried out using Eq. 2 to evaluate the dispersion state and the diameter of SiO_2

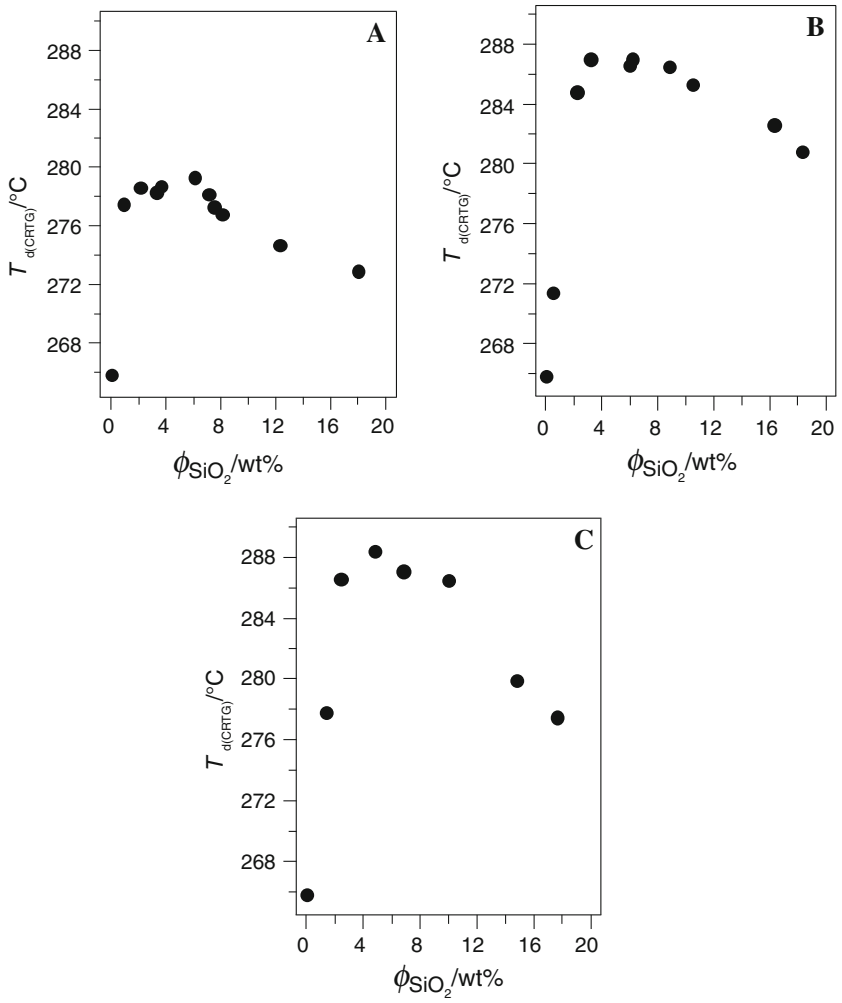

Fig. 2 Relationship between decomposition temperature ($T_{d(CRTG)}$) and mass fraction (ϕ_{SiO_2}) of PMMA–SiO_2 composites (23 nm) (**a**), PMMA–SiO_2 composites (17 nm) (**b**), and PMMA–SiO_2 composites (13 nm) (**c**)

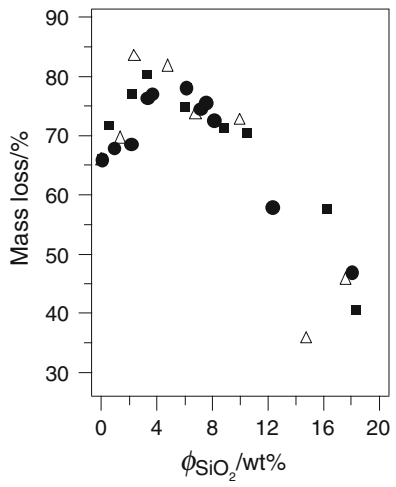

Fig. 3 Relationship between relative mass loss occurred in the first step of degradation and mass fraction (ϕ_{SiO_2}) of PMMA–SiO_2 composites (23 nm) (*circle*), PMMA–SiO_2 composites (17 nm) (*square*), and PMMA–SiO_2 composites (13 nm) (*triangle*)

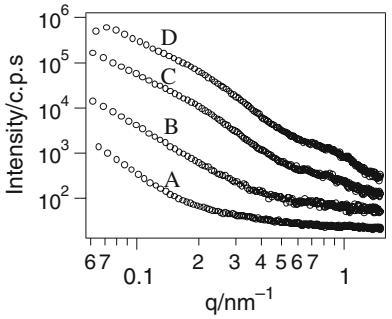

Fig. 4 SAXS profiles of PMMA and PMMA–SiO_2 (17 nm) composites with various mass fraction of SiO_2. *A* PMMA, *B* 1%, *C* 4%, *D* 15%

particles. The obtained diameter of SiO_2 particle was 16 nm for PMMA–SiO_2 composites (17 nm) with 4 and 15 wt% of ϕ_{SiO_2} under the condition of fixed $f(R) = 0.1$. These results indicated that SiO_2 particles dispersed homogeneously in PMMA in the ϕ_{SiO_2} range below 15 wt%. The SAXS profile

of PMMA–SiO_2 composites with 15 wt% accompanied the scattering at lower q region, which indicated the existence of SiO_2 aggregation. PMMA–SiO_2 composites with ϕ_{SiO_2} below 10 wt% were optically transparent; however, the composites became opaque with the increase in ϕ_{SiO_2} above 15 wt% as a result of particle aggregation.

From SAXS, measurements indicated the homogeneous SiO_2 dispersion in PMMA for the composites below 15 wt%. The number of PMMA molecules per one SiO_2 particle was evaluated for PMMA–SiO_2 composites at ϕ_{SiO_2}, where the maximum $T_{d(CRTG)}$ obtained, using the density 1.2 g cm^{-3} for PMMA and 2.2 g cm^{-3} for SiO_2. The number of PMMA molecules per one SiO_2 particle was 1800 (23 nm, 6 wt%), 750 (17 nm, 3 wt%), and 300 (13 nm, 5 wt%).

The radius of gyration (R_g) of PMMA used in this experiment was evaluated from the repeating unit length (l) and the degree of polymerization (n).

$$R_g = \frac{\sqrt{nl^2}}{\sqrt{6}} = 4.2(\text{nm}) \quad (5)$$

R_g obtained by Eq. 5 is the size of one PMMA molecule without any restrictions. The real PMMA molecules have various restrictions such as entanglement, intermolecular interaction, and outer stress. On the other hand, the real radius of one PMMA molecule estimated from the density (1.2 g cm^{-3}) was 3.4 nm. The average diameter of one random PMMA molecule was about 7 nm, which was smaller than that of SiO_2 particles. With decreasing the SiO_2 particle size and closing to the PMMA molecular size, the curvature of surface increased and the number of PMMA molecules absorbed on the SiO_2 particle surface became smaller.

The distance between the closed SiO_2 particles were 80 (23 nm, 6 wt%), 63 (17 nm, 3 wt%), and 45 (13 nm, 5 wt%) nm by assuming the homogenous distribution of SiO_2 particles like hexagonal packing. These distances corresponded to 6–12 PMMA molecules with entanglements between the surfaces of closest SiO_2 particles. For the PMMA–SiO_2 (17 nm) composites with 15 wt%, the distance between the closed SiO_2 particles became 37 nm, which corresponded to the size of four PMMA molecules between the surfaces of SiO_2 particles. Further addition of SiO_2 particles, the number of PMMA molecules between SiO_2 particles became smaller to keep the homogeneous distribution. In other words, SiO_2 particles dispersed accompanied with one layer of PMMA molecules absorbed on the surface under the condition of homogeneous distribution. SiO_2 particles preferred to aggregate by the geometrical restriction in the ϕ_{SiO_2} range above 15 wt%.

IR spectra of SiO_2 particle surface after heating to 125 °C indicated the co-existence of hydrogen bonded hydroxyl (OH) groups and isolated OH groups, which appeared as a broad peak at around 3400 cm^{-1} and a week sharp peat at 3750 cm^{-1}, respectively. No direct evidence of hydrogen bond formation between OH groups in SiO_2 surface and carbonyl groups in PMMA was observed by IR measurement.

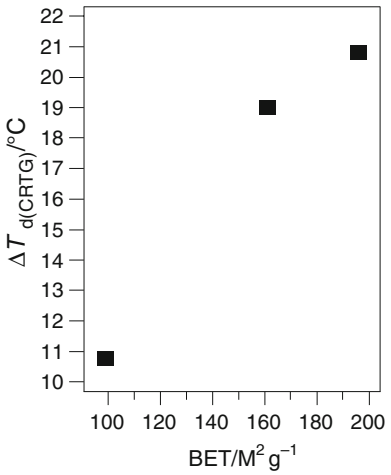

Fig. 5 Relationship between the decomposition temperature ($T_{d(CRTG)}$) improvement of PMMA–SiO_2 composites (2 wt%) and specific surface area of SiO_2

The $T_{d(CRTG)}$ values were plotted against the specific surface area of SiO_2 for PMMA–SiO_2 composites with 2 wt% of ϕ_{SiO_2} in Fig. 5. Under this ϕ_{SiO_2} condition, the homogeneous dispersion of SiO_2 particles was conformed by SAXS measurement. $T_{d(CRTG)}$ increased almost linearly with the specific surface area of SiO_2. The highest specific surface area, which corresponded to the 13 nm SiO_2 particles, showed a slightly smaller $T_{d(CRTG)}$ value from the linear relationship. The number of PMMA molecules absorbed on one SiO_2 particle of 13 nm was smaller that those for larger SiO_2 particles. The result shown in Fig. 5 indicated that the absorption of PMMA molecules on SiO_2 particle by the hydrogen bond formation between hydroxyl group of SiO_2 particles and carbonyl group in PMMA improved the thermal stability of PMMA.

Thermal stability of PMMA molecules absorbed on SiO_2 particle surface is higher than normal PMMA due to the reduced molecular mobility. With decreasing the particle size the number of PMMA molecules absorbed on SiO_2 particle surface decreased due to the increase in curvature, especially in the case of particle size closed to PMMA molecular size. From the assumption of closed packed model and the average diameter of one random PMMA molecule (7 nm), the number of PMMA molecules absorbed on SiO_2 particle surface were estimated. At the fixed ϕ_{SiO_2}, the number of particles increased with the decrease in particle size. The number of PMMA molecules per one SiO_2 particle was also estimated from the densities of PMMA and SiO_2 particle at 2 wt%. Then the number of

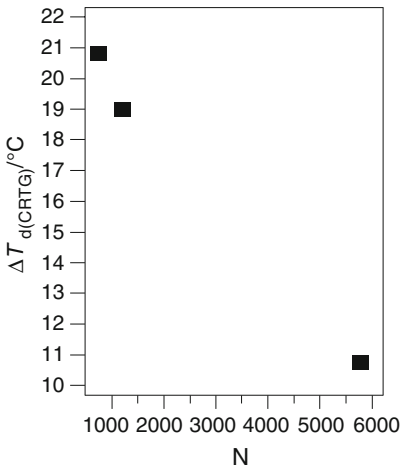

Fig. 6 Relationship between the decomposition temperature ($T_{d(CRTG)}$) improvement of PMMA–SiO_2 composites (2 wt%) and the number of PMMA molecules free from SiO_2 surface

non-absorbed PMMA molecules per one SiO_2 particle (N) was obtained. $T_{d(CRTG)}$ was plotted against the estimated N in Fig. 6. $T_{d(CRTG)}$ decreased with the increase in PMMA molecules free from the SiO_2 particle surface. As described above, 6–12 PMMA molecules existed between the closed SiO_2 particles at the ϕ_{SiO_2}, where the maximum $T_{d(CRTG)}$ was obtained. The absorption of PMMA on SiO_2 particle surface influenced the thermal stability of 3–6 PMMA molecules which were free from the surface of SiO_2 particles. The structure analysis of multi-layers of amphiphilic di-block copolymer prepared on Si wafer by Langmuir–Blodgett method indicated that the effect of Si surface on the layer structure appeared until eight layers [10, 11]. For PMMA–SiO_2 composites, the PMMA molecule absorbed on SiO_2 surface influenced the thermal stability of few PMMA molecules trough molecular entanglements.

Conclusions

Regarding the CRTG results for PMMA and PMMA–SiO_2 nano-composite with different size SiO_2 with various particle sizes, the dispersed SiO_2 inhibited the thermal degradation of PMMA. The improvement efficiency on thermal stability depended on the dispersion state of SiO_2 nano-particles and the size of SiO_2 particles. The degradation improvement increased with increasing the specific surface area of SiO_2 particles due to the decrease in PMMA molecules free from the trapping on SiO_2 particle surface.

References

1. Chang T, Wang Y, Hong Y, Chen H. Effect of interfacial structure on the thermal stability of poly(methyl methacrylate)-silica hybrids. Thermochim Acta. 2003;397:219–226.
2. Kashiwagi T, Morgan A, Antonucci J, van Landingham M, Harris R, Awad W. Thermal and flammability properties of a silica poly(methylmethacrylate) nanocomposite. J Appl Polym Sci. 2003;89:2072–2078.
3. Yang Y, Dan Y. Preparation of PMMA/SiO2 composite particles via emulsion polymerization. Colloid Polym Sci. 2003;281:794–799.
4. Katsikis N, Zahradnik F, Helmschrott A, Münstedt HA, Vital A. Thermal stability of poly(methyl methacrylate)/silica nano- and microcomposites as investigated by dynamic-mechanical experiments". Polym Degrad Stab. 2007;92:1966–1976.
5. García N, Corrales T, Guzmán J, Tiemblo P. Understanding the role of nanosilica particle surfaces in the thermal degradation of nanosilicaepoly(methyl methacrylate) solution-blended nanocomposites: from low to high silica concentration. Polym Degrad Stab. 2007;92:635–643.
6. Castrillo PD, Olmos D, Amador DR, González-Benito J. Real dispersion of isolated fumed silica nanoparticles in highly filled PMMA prepared by high energy ball milling. J Colloid Interface Sci. 2007;308:318–324.
7. Wang H, Meng S, Xu P, Zhong W, Du Q. Effect of traces of inorganic content on thermal stability of poly(methyl methacrylate) nanocomposites. Polym Eng Sci. 2007;47:302–307.
8. Zou DQ, Yoshida H. Effect of silica nanoparticles on thermal decomposition of polymethacrylate esters. Polym Prepr Jpn. 2008;57:822.
9. Hamly IW, Castelletto V. Small-angle scattering of block copolymer: in the melt, solution and crystal state. Prog Polym Sci. 2004;29:909–948.
10. Yamada T, Jung SY, Yoshida H. Structure analysis of amphiphilic di-block copolymer monolayer by X-ray reflectivity. J Phys Conf Ser. 2007;83:012005.
11. Yamada T, Jung SY, Yoshida H. Analysis of multi layer structure of amphiphilic di-block copolymer by X-ray reflectivity. J Phys Conf Ser. 2007;83:012017.